JACS
JOURNAL OF THE AMERICAN CHEMICAL SOCIETY
Article
pubs.acs.org/JACS

Toward Tetraradicaloid: The Effect of Fusion Mode on Radical Character and Chemical Reactivity

Pan Hu,[†] Sangsu Lee,[‡] Tun Seng Herng,[§] Naoki Aratani,[∥] Théo P. Gonçalves,[⊥] Qingbiao Qi,[†] Xueliang Shi,[†] Hiroko Yamada,[∥] Kuo-Wei Huang,[⊥] Jun Ding,*[,§] Dongho Kim,*[,‡] and Jishan Wu*[,†,#]

[†]Department of Chemistry, National University of Singapore, 3 Science Drive 3, Singapore 117543, Singapore

[‡]Spectroscopy Laboratory for Functional π-Electronic Systems and Department of Chemistry, Yonsei University, Seoul 120-749, Korea

[§]Department of Materials Science & Engineering, National University of Singapore, Singapore 119260, Singapore

[∥]Graduate School of Materials Science, Nara Institute of Science and Technology (NAIST), 8916-5 Takayama-cho, Ikoma 630-0192, Japan

[⊥]Division of Physical Science and Engineering and KAUST Catalysis Center, King Abdullah University of Science and Technology (KAUST), Thuwal 23955-6900, Kingdom of Saudi Arabia

[#]Institute of Materials Research and Engineering, A*STAR, 2 Fusionopolis Way, Innovis, #08-03, Singapore 117602, Singapore

Supporting Information

ABSTRACT: Open-shell singlet diradicaloids display unique electronic, nonlinear optical, and magnetic activity and could become novel molecular materials for organic electronics, photonics, and spintronics. However, design and synthesis of diradicaloids with a significant polyradical character is a challenging task for chemists. In this Article, we report our efforts toward a tetraradicaloid system. A series of potential tetraradicaloids by fusion of two *p*-quinodimethane (*p*-QDM) units with naphthalene or benzene rings in different modes were synthesized. Their model compounds containing one *p*-QDM moiety were also prepared and compared. Their ground-state structures, physical properties, and chemical reactivity were systematically investigated by various experimental methods such as steady-state and transient absorption, two-photon absorption, X-ray crystallographic analysis, electron spin resonance, superconducting quantum interference device, and electrochemistry, assisted by density functional theory calculations. It was found that their diradical and tetraradical characters show a clear dependence on the fusion mode. Upon the introduction of more five-membered rings, the diradical characters greatly decrease. This difference can be explained by the pro-aromaticity/antiaromaticity of the molecules as well as the intramolecular charge transfer. Our comprehensive studies provide a guideline for the design and synthesis of stable open-shell singlet polycyclic hydrocarbons with significant polyradical characters.

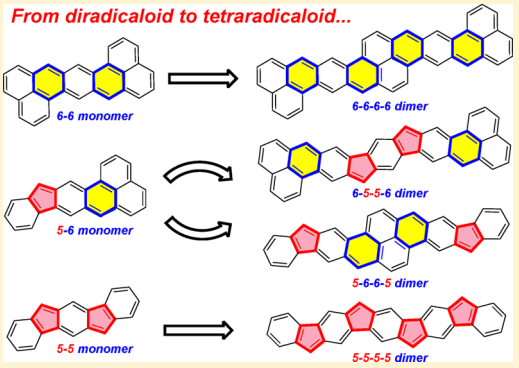

I. INTRODUCTION

π-Conjugated polycyclic hydrocarbons (PHs) with an open-shell singlet diradical ground state have recently attracted tremendous interest due to their unique electronic, optical, and magnetic properties and potential applications in organic electronics, nonlinear optics, spintronics, and energy storage devices.[1] According to broken symmetry density functional theory (DFT) calculations, any molecule with a nonzero diradical character in the ground state can be classified as a diradicaloid (diradical-like molecule). So far, various relatively stable PH-based open-shell singlet diradicaloids have been synthesized, for example, bisphenalenyls,[2] zethrenes,[3] indenofluorenes,[4] anthenes,[5] and quinoidal rylenes.[6] Fundamental studies on the structure−diradical character−physical property relationships have revealed that both the aromaticity and the steric strain played important roles in determining the ground-state electronic structure and physical property. The next natural target is to access stable open-shell singlet tetraradicaloids or even polyradicaloids, which may open the opportunities to investigate multiple spin interactions and molecular magnetism. However, this is a very challenging task for chemists because molecules with significant tetraradical character or polyradical character are supposed to be extremely reactive. In addition, the multiple radical character is also dependent on the interactions between individual spins; that is, too strong or too weak bonding interaction between the spins may result in too low or too high multiple radical character, respectively. Therefore, one must carefully tune the structures to reach a balance.

Tobe's group recently synthesized a potential tetraradicaloid hydrocarbon, the cyclic tetracyclopenta[*def*,*jkl*,*pqr*,*vwx*]-

Received: December 1, 2015
Published: December 30, 2015

DOI: 10.1021/jacs.5b12532
J. Am. Chem. Soc. 2016, 138, 1065−1077

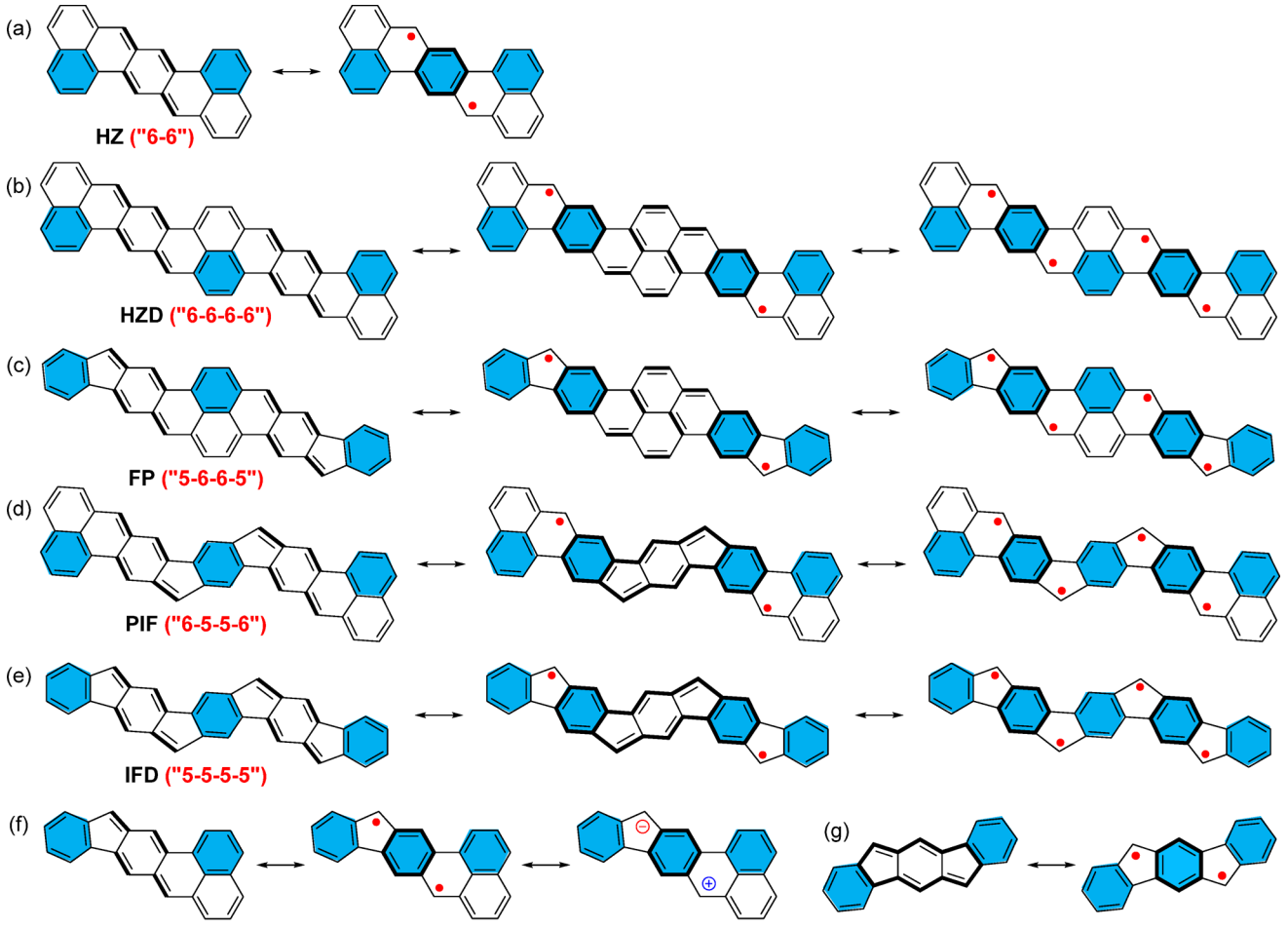

Figure 1. Resonance structures of the studied diradicaloid and tetraradicaloid systems with different fusion modes.

tetraphenylene (TCPTP). However, all experimental evidence implies that TCPTP is better described as a singlet diradicaloid with a moderate diradical character (y_0 = 0.258) and a small tetraradical character (y_1 = 0.085, calculated by the LC-UBLYP/6-311+G(d,p) method based on the crystallographic structure).[7] Our particular interest here is to synthesize and study the properties of a series of linear tetraradicaloids. Because our group previously reported several derivatives of the pro-aromatic heptazethrene (**HZ**) with moderate diradical characters (Figure 1a),[3d,e,g] we first attempted to synthesize the fused heptazethrene dimer **HZD** (Figure 1b), which could exhibit both diradical and tetraradical characters. This sounds reasonable because from the closed-shell form to the diradical form and to the tetraradical form, one additional aromatic sextet ring (the hexagon highlighted in blue color) is gained, which can serve as the driving force to be open-shell diradical/tetraradical (Figure 1b). However, our results show that the target compounds, even after appropriate kinetic and thermodynamic stabilization, are so reactive and cannot be isolated and characterized. To obtain more stable tetraradicaloids, we hypothesized that this can be done by introduction of two cyclopenta- rings to the molecular backbone because it was reported that many cyclopenta-fused polycyclic aromatic hydrocarbons (PAHs) are highly stable.[8] We proposed two different fusion modes: in one case, the two outmost phenalenyl units in **HZD** are replaced by two indenyl moieties, resulting in a bis-fluoreno-pyrene structure **FP** (Figure 1c); in the other case, the central pyrene moiety in the **HZD** is replaced by an antiaromatic *s*-indacene unit, leading to a bis-phenaleno-indenofluorene structure **PIF** (Figure 1d). Depending on whether it is a six-membered ring or a five-membered ring linkage between the *para*-quinodimethane (*p*-QDM) and the aromatic benzene or naphthalene units, the **HZD**, **FP**, and **PIF** can be classified as 6-6-6-6, 5-6-6-5, and 6-5-5-6 fusion modes, respectively. For comparison, the derivatives of the linearly fused indenofluorene dimer **IFD** with a 5-5-5-5 fusion mode were also synthesized (Figure 1e).[9] It is interesting to see that the ground-state reactivity showed a strong dependence on the molecular fusion mode. For better understanding of the difference between fusion modes, three types of model compounds were prepared too, the heptazethrene **HZ** with a 6-6 fusion mode (Figure 1a), the phenalenofluorene **PF** with a 6-5 fusion mode (Figure 1f), and the indenofluorene **IF** with a 5-5 fusion mode (Figure 1g). Their ground states and physical properties were systematically investigated by various experimental methods such as steady-state and transient absorption (TA), two-photon absorption (TPA), X-ray crystallographic analysis, electron spin resonance (ESR), superconducting quantum interference device (SQUID), and electrochemistry, assisted by DFT calculations.

II. RESULTS AND DISCUSSION

1. 6-6-6-6 System (HZD). The fused heptazethrene dimers were synthesized via an intramolecular Friedel−Crafts alkylation followed by oxidative dehydrogenation strategy (Scheme 1). The building block **1** was first obtained by Suzuki

DOI: 10.1021/jacs.5b12532
J. Am. Chem. Soc. 2016, 138, 1065−1077

Scheme 1. Synthesis of Heptazethrene Dimers HZD-M and HZD-F[a]

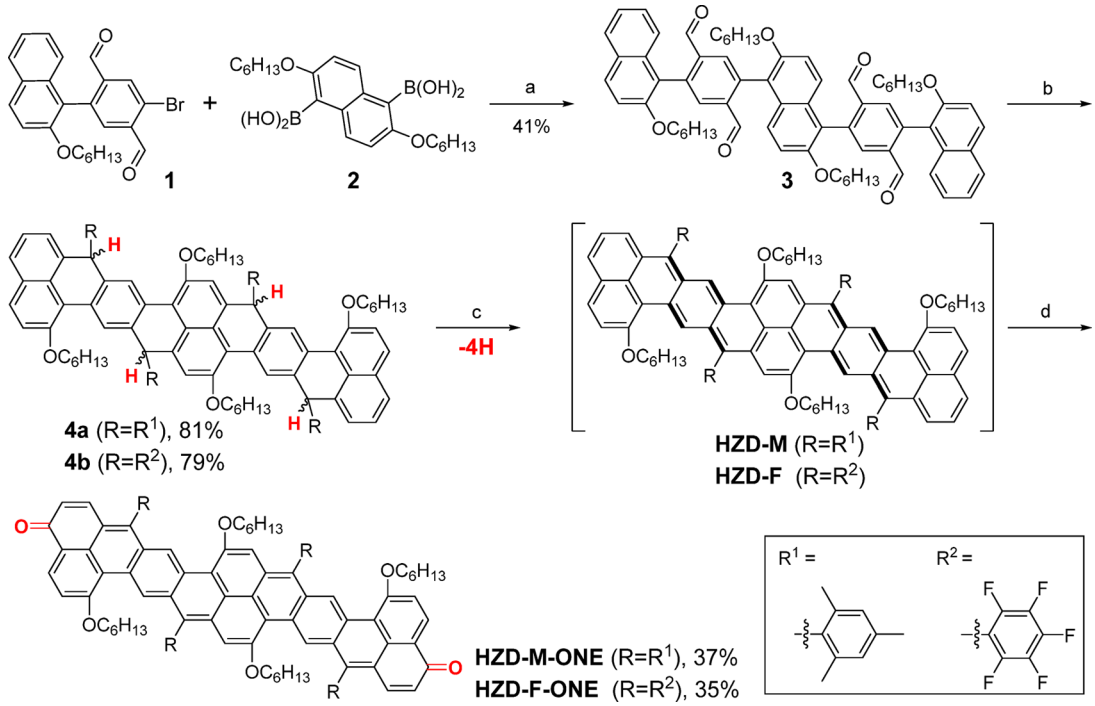

[a]Reagents and conditions: (a) $Pd(PPh_3)_4$, 2 M K_2CO_3, toluene/ethanol, 105 °C, 12 h; (b) (i) ArMgBr, Ar = mesityl or pentafluorophenyl, dry THF, rt, 12 h, (ii) $BF_3{\cdot}OEt_2$, dry DCM, rt, 5 min; (c) DDQ, dry toluene, rt; (d) work up in air.

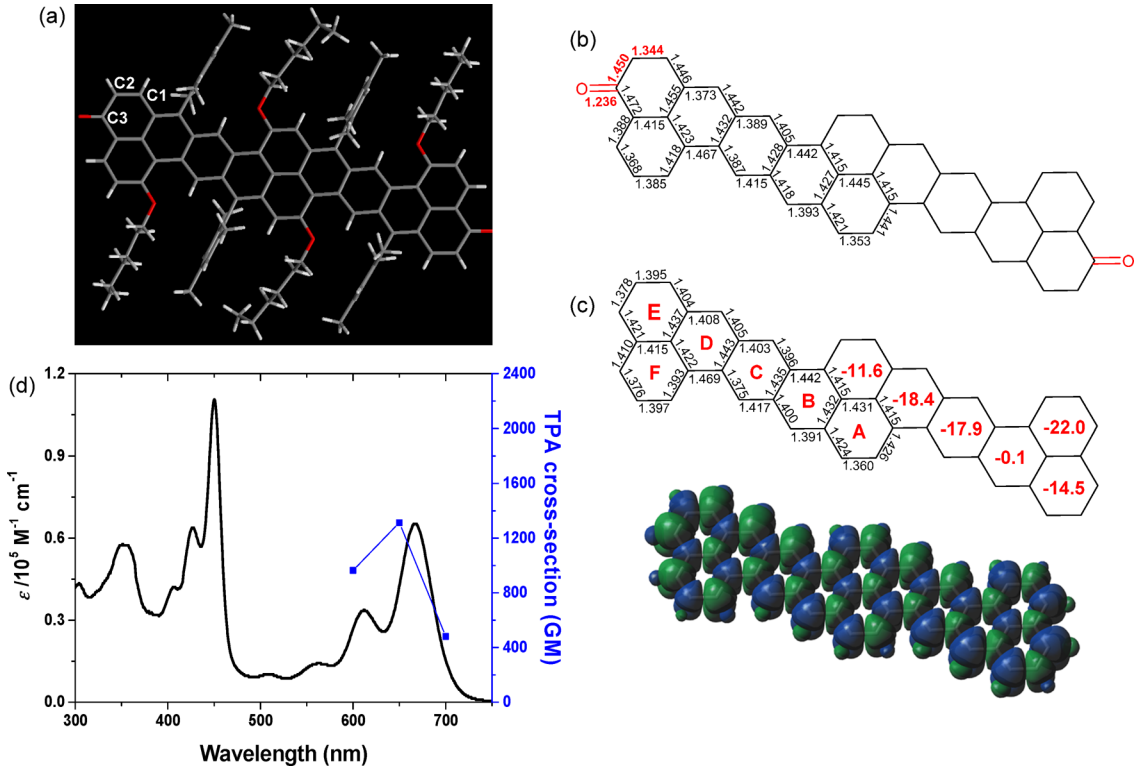

Figure 2. (a) X-ray crystallographic structure of **HZD-M-ONE**; (b) selected bond lengths of the backbone of **HZD-M-ONE**; (c) calculated (UCAM-B3LYP) bond lengths, NICS(1)zz values, and spin density distribution of the singlet diradical of parent **HZD**; and (d) one-photon and two-photon absorption spectra of **HZD-M-ONE**. TPA spectra are plotted at $\lambda_{ex}/2$.

coupling between 2,5-dibromobenzene-1,4-dicarboxaldehyde and (2-(hexyloxy)naphthalen-1-yl)boronic acid (see the Supporting Information). Suzuki coupling between **1** and (2,5-bis(hexyloxy)-1,4-phenylene)diboronic acid (**2**) gave the key intermediate tetraaledhyde **3**. The alkoxy chain was introduced to improve the solubility and also prevent the

DOI: 10.1021/jacs.5b12532
J. Am. Chem. Soc. 2016, 138, 1065−1077

formation of five-membered ring containing isomers in the coming cyclization step. Treatment of **3** with mesitylmagnesium bromide or pentafluorophenylmagnesium bromide afforded the corresponding tetraol compounds, which were subjected to $BF_3{\cdot}OEt_2$-mediated Friedel–Crafts alkylation reaction to give the tetrahydro- precursors **4a**/**b**. The dehydrogenation of precursor **4a**/**b** was conducted by treatment with 2,3-dichloro-5,6-dicyano-1,4-benzoquinone (DDQ) in dry toluene at room temperature. However, this gave a quite reactive species (**HZD-M** and **HZD-F**), which could transform into the dioxo- compounds **HZD-M-ONE** and **HZD-F-ONE** (dark green solid) in 1 h. Workup and purification of the reaction mixture in air afforded compounds **HZD-M-ONE** and **HZD-F-ONE**, respectively. The structures of **HZD-M-ONE**/**HZD-F-ONE** were unambiguously identified by NMR, high-resolution mass spectrometry (see the Supporting Information), and X-ray crystallographic analysis.

The X-ray crystallographic structure of **HZD-M-ONE** clearly disclosed a nearly planar molecular backbone, with the ketone groups formed at the *peri*- positions of the terminal naphthalene rings (Figure 2a).[10] Bond length analysis of the backbone revealed a new PAH structure containing 10 benzenoid rings, fused by two α,β-unsaturated ketone moieties (C1–C2, 1.344 Å; C2–C3, 1.450 Å; C3–O, 1.236 Å) (Figure 2b).

Broken symmetry DFT calculations (UCAM-B3LYP/6-31G(d,p)) were conducted to study the ground-state electronic structure and to understand the high reactivity of **HZD**. The singly occupied molecular orbital (SOMO) profiles of the α and β spins showed an obvious disjoint feature, indicating a large diradical character (Figure S1). Indeed, a large diradical character (y_0 = 0.713) was calculated, but the tetraradical character (y_1 = 0.009) turned out to be very small (Table 1). A small singlet–triplet energy gap (ΔE_{S-T} = −3.0 kcal/mol) was predicted. The large diradical character explains the very high chemical reactivity of **HZD-M** and **HZD-F**, although they are stabilized by bulky mesityl groups (in **HZD-M**) or electron-deficient pentafluorophenyl groups (in **HZD-F**). The calculated bond lengths and NICS(1)zz values of the ground-state singlet diradical indicate large aromatic character for the rings A–C and E,F, implying a large contribution of the diradical form to the ground-state structure. On the other hand, ring D has nonaromatic character (Figure 2c). The spin densities are evenly distributed throughout the whole π-conjugated backbone, and high spin density can be found at the *peri*- positions of the terminal naphthalene units (Figure 2c), which can explain why oxygen addition preferred to take place at these sites to generate the dioxo-products. The other reactive sites are kinetically blocked to a certain extent. We also attempted to conduct ESR measurements on the in situ generated **HZD-M** in a sealed ESR tube under nitrogen atmosphere. However, because of the high reactivity of this compound, it cannot be directly determined during the dehydrogenation reaction. An intense single-line ESR signal (g_e = 2.00280) was observed after adding the DDQ in 10 min (Figure S8). The variable temperature (VT) ESR measurements on the solid sample after removing the solvent under nitrogen showed that the ESR intensity (I) increased with decreasing temperature (T), with I being approximately proportional to $1/T$ (Figure S8), indicating that the major magnetically active species in the mixture is a monoradical intermediate rather than the diradical, which may be due to the high reactivity and the short lifetime of **HZD-M**. Experiments by using in situ generated **HZD-F** gave similar results.

Table 1. Calculated (UCAM-B3LYP) Diradical Character (y_0), Tetraradical Character (y_1), and Singlet–Triplet Energy Gap (ΔE_{S-T}) for the Parent Systems

fusion mode	compd	y_0	y_1	ΔE_{S-T} (kcal/mol)
6-6-6-6	HZD	0.713	0.009	−3.0
5-6-6-5	FP	0.635	0.003	−2.3
6-5-5-6	PIF	0.351	0.031	−4.2
5-5-5-5	IFD	0.038	0.005	−8.4
6-6	HZ	0.17		−8.1
6-5	PF	0.05		−9.1
5-5	IF	0.00		−13.2

The two dioxo- products **HZD-M-ONE**/**HZD-F-ONE** exhibit deep green color in both solid and solution phases. Their one-photon absorption spectra (OPA) in dichloromethane (DCM) are shown in Figure 2d and Figure S12, and the data are summarized in Table 2. Compound **HZD-M-ONE** solution displays a well-resolved spectrum with the absorption maximum at 667 nm (ε = 6580 M^{-1} cm^{-1}) (Figure 1d and Table 2), which can be correlated to the HOMO → LUMO transition (λ_{abs} = 688 nm, oscillator strength f = 0.7071) on the basis of time-dependent (TD) DFT calculations (B3LYP/6-31G*) (see the Supporting Information). Compound **HZD-F-ONE** with a different substituent group at the bay region shows an absorption spectrum similar to that of **HZD-M-ONE** (Figure S12). The excited-state dynamics of compounds **HZD-M-ONE**/**HZD-F-ONE** were investigated by femtosecond transient absorption (TA) measurements (Figure S9). The two compounds exhibit similar TA spectra with two ground-state bleaching (GSB) signals around 645 and 714 nm as well as a weak excited-state absorption (ESA) band in 450–630 nm. The singlet excited-state lifetimes (τ) of **HZD-M-ONE** and **HZD-F-ONE** were determined to be 2.9 and 2.5 ns, respectively. These singlet excited-state lifetimes are similar to those of typical fused PAHs. Because of the largely extended π-conjugation, they are expected to exhibit remarkable hyperpolarizability. Therefore, two-photon absorption (TPA) measurements were conducted for these two compounds by the Z-scan method in the wavelength range from 1200 to 1400 nm, where one-photo absorption (OPA) contribution is negligible (Figure 1d and Figure S10). Compound **HZD-M-ONE** exhibited a remarkable TPA cross-section maximum ($\sigma^{(2)}{}_{max}$) value of 1300 GM at 1300 nm, which is slightly smaller than that of compound **HZD-F-ONE** ($\sigma^{(2)}{}_{max}$ = 1400 GM at 1300 nm) (Figure S10). Cyclic voltammetry (CV) and differential pulse voltammetry (DPV) were conducted to study the electrochemical properties of compounds **HZD-M-ONE**/**HZD-F-ONE** (Figure S11 and Table 2). Compound **HZD-M-ONE** showed two reversible oxidation waves at $E_{1/2}{}^{ox}$ = 0.14, 0.72 V and two reversible reduction waves at $E_{1/2}{}^{red}$ = −1.67, −2.27 V (vs Fc/Fc^+, Fc = ferrocene), while **HZD-F-ONE** showed one quasi-reversible oxidation wave at $E_{1/2}{}^{ox}$ = 0.55 V and two reversible reduction waves at $E_{1/2}{}^{red}$ = −1.39 and −1.95 V. The electrochemical energy gaps were calculated as 1.63 and 1.77 eV for **HZD-M-ONE** and **HZD-F-ONE**, respectively, which are consistent with their optical energy band gaps (Table 2).

2. 6-5-5-6 (FP) and 5-6-6-5 (PIF) Systems. To obtain more stable materials, two cyclopenta rings were introduced, and the syntheses of derivatives of the 5-6-6-5 fused **PF** and the

DOI: 10.1021/jacs.5b12532
J. Am. Chem. Soc. 2016, 138, 1065–1077

Table 2. Photophysical and Electrochemical Data of the Tetraradicaloids and Model Compounds[a]

compd	λ_{abs} (nm)	ε_{max} (M^{-1} cm^{-1})	τ (ps)	$\sigma^{(2)}_{max}$ (GM)	$E_{1/2}^{ox}$ (V)	$E_{1/2}^{red}$ (V)	HOMO (eV)	LUMO (eV)	E_g^{EC} (eV)	E_g^{opt} (eV)
HZD-M-ONE	450	11 050	20 (t_1)	1300[b]	0.14	−1.67	−4.86	−3.23	1.63	1.75
	667	6580	2900 (t_2)		0.72	−2.27				
	612	3380								
HZD-F-ONE	446	76 220	2450	1400[b]	0.55	−1.39	−5.3	−3.53	1.77	1.83
	643	52 790				−1.95				
	591	28 210								
FP-M	836	50 750	25	1500[c]	−0.26	−1.45	−4.41	−3.47	0.94	1.10
	960	6510			−0.05	−1.65				
	1005	9860			0.39	−1.84				
	1096	1550			0.67	−2.37				
PIF-M-ONE	355	56 060	7.2	770[b]	0.49	−1.41	−5.09	−3.54	1.57	1.85
	620	41 260			0.95	−1.59				
PIF-F-ONE	357	51 870	2.2	970[b]	0.92	−1.00	−5.65	−3.87	1.78	1.83
	625	36 530				−1.19				
						−1.99				
IFD-CF_3	367	53 320	0.7 (t_1)	800[d]	0.49	−1.01	−5.25	−3.88	1.37	1.39
	662	23 680	3.7 (t_2)		0.74	−1.23				
	722	41 420								
HZ-M	327	36 590	55 (t_1)	730[e]	−0.27	−2.03	−4.47	−2.87	1.60	1.91
	613	70 030	5500 (t_2)		0.17	−2.36				
HZ-F	326	25 220	80 (t_1)	900[e]	0.07	−1.67	−4.8	−3.23	1.57	1.90
	610	42 180	5100 (t_2)		0.47	−2.09				
PF-M	436	12 440	7.2	400[b]	−0.07	−1.87	−4.65	−3.03	1.62	1.56
	627	6760			0.62	−2.37				
PF-F	436	12 440	7.2	410[b]	0.25	−1.43	−4.98	−3.49	1.49	1.43
	627	6760			0.77	−1.97				
IF-M	515	42 640	0.7 (t_1)		0.71	−1.56	−5.41	−3.32	2.09	2.21
			14 (t_2)			−2.07				
IF-CF_3	541	11 530	0.6		0.89	−1.14	−5.64	−3.75	1.89	2.16
						−1.48				

[a] λ_{abs}: absorption maximum. ε_{max}: molar extinction coefficient at the absorption maximum. τ is the singlet excited-state lifetime obtained from TA in toluene. $E_{1/2}^{ox}$ and $E_{1/2}^{red}$ are half-wave potentials of the oxidative and reductive waves, respectively, with potentials vs Fc/Fc^+ couple. HOMO and LUMO energy levels were calculated according to equations: HOMO = $-(4.8 + E_{ox}^{onset})$ and LUMO = $-(4.8 + E_{red}^{onset})$, where E_{ox}^{onset} and E_{red}^{onset} are the onset potentials of the first oxidative and reductive redox wave, respectively. E_g^{EC}: electrochemical energy gap derived from LUMO−HOMO. E_g^{Opt}: optical energy gap derived from the lowest energy absorption onset in the absorption spectra. [b] $\sigma^{(2)}_{max}$ is the maximum TPA cross section at the wavelength of 1300 nm. [c] $\sigma^{(2)}_{max}$ is the maximum TPA cross section at the wavelength of 1700 nm. [d] $\sigma^{(2)}_{max}$ is the maximum TPA cross section at the wavelength of 1500 nm. [e] $\sigma^{(2)}_{max}$ is the maximum TPA cross section at the wavelength of 1200 nm measured in DCM.

6-5-5-6 fused **PIF** were attempted. Similarly, bulky mesityl (in **PF-M** and **PIF-M**) or electron-withdrawing pentafluorophenyl (in **PF-F** and **PIF-F**) substituents were attached to the most reactive sites. The synthetic route for these compounds is shown in Scheme 2. Suzuki coupling of 2,5-dibromobenzene-1,4-dicarboxaldehyde with phenylboronic acid gave the key building block **5** in good yield (see the Supporting Information). The key intermediate tetraaldehyde **6** was obtained by Suzuki coupling between **5** and the boronic acid **2**. Compound **6** then was treated with mesitylmagnesium bromide/pentafluorophenylmagnesium bromide followed by an intramolecular Friedel−Crafts alkylation reaction to afford the tetrahydro- precursors **7a**/**7b**. Compound **FP-M** was finally obtained as a dark green solid by oxidative dehydrogenation of **7a** with DDQ at 80 °C for one-half an hour. However, the pentafluorophenyl-substituted compound **7b** could not be dehydrogenated by DDQ even under reflux in toluene. This may be due to the very strong electron-withdrawing nature of pentafluorophenyl group. The synthesis of **PIF-M**/**PIF-F** tetrahydro-precursors **10a**/**10b** followed a strategy similar to the synthesis of **7a**/**7b**, but starting from the tetra-aldehyde intermediate **9** (Scheme 2). Similar to the **HZD-M**/**HZD-F** compounds, the dehydrogenation of **10a**/**10b** only gave the dioxo- product **PIF-M-ONE**/**PIF-F-ONE** instead of the target **PIF-M**/**PIF-F** compounds. The structures of **FP-M**, **PIF-M-ONE**, and **PIF-F-ONE** were identified unambiguously by NMR spectroscopy, high-resolution mass spectrometry, and crystallographic analysis (vide infra, and Supporting Information).

Compound **FP-M** only shows a broadened ^1H NMR spectrum in solution even at low temperature (down to −100 °C, Figure S13). **FP-M** in DCM exhibits a broad three-line ESR signal with g_e = 2.0027 (Figure 3a), and the signal intensity gradually decreases as temperature decreases, indicating a singlet diradical ground state (Figure S14). The SQUID measurement was conducted to study the temperature-dependent magnetic susceptibility behavior. The results show that its magnetic susceptibility increases as temperature increases after 100 K, which further implies a singlet ground state for **FP-M** compound (Figure 3b). The singlet−triplet energy gap ($2J/k_B$, i.e., ΔE_{S-T}) was calculated to be −852.6 K (−1.69 kcal/mol) for **FP-M** by a careful fitting of the data using the Bleaney−Bowers equation (Figure 3b).[11] To further understand the magnetic properties of **PIF-M**, the in situ

DOI: 10.1021/jacs.5b12532
J. Am. Chem. Soc. 2016, 138, 1065−1077

Scheme 2. Synthesis of FP-M/FP-F and PIF-M/PIF-F[a]

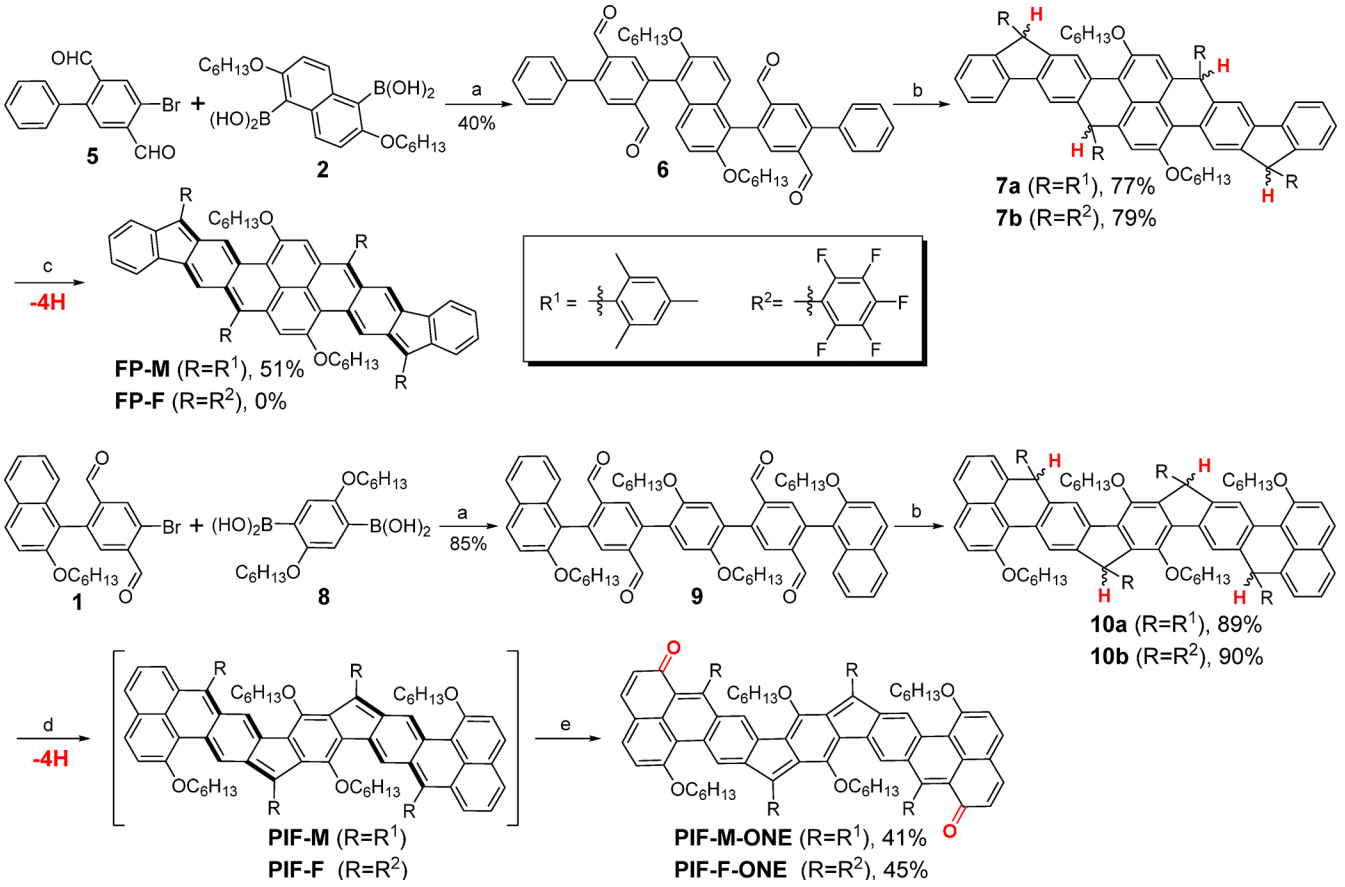

[a]Reagents and conditions: (a) $Pd(PPh_3)_4$, 2 M K_2CO_3, toluene/ethanol, 105 °C; (b) (i) ArMgBr, Ar = mesityl or pentafluorophenyl, dry THF, rt, 12 h, (ii) $BF_3{\cdot}OEt_2$, dry DCM, rt, 5 min; (c) DDQ, dry toluene, 80 °C, 30 min; (d) DDQ, dry toluene, rt; (e) work up in air.

ESR test was also conducted. However, similar to **HZD-M**, only monoradical species were detected during the test. More specifically, the VT ESR measurements on the solid sample after removing the solvent under nitrogen showed that the ESR intensity (I) increased as temperature (T) decreased, with I being approximately proportional to $1/T$ (Figure S8), indicating the formation of the monoradical intermediates presumably due to extremely high reactivity of the diradical species.

Single crystals suitable for crystallographic analysis were obtained for **FP-M**[12] and **PIF-M-ONE**[13] by solvent diffusion methods, and their structures are shown in Figure 4. **FP-M** shows a slightly twisted structure due to the steric congestion at the cove region (Figure 4a). Bond length analysis reveals that the length of the C1−C2 bond (1.400 Å) is significantly longer than that of the typical olefins (1.33−1.34 Å), but is much shorter than a typical $C(sp^2)-C(sp^2)$ single bond (~1.45 Å), indicating a large contribution of the diradical form to the ground-state electronic structure (Figure 4b). DFT calculations (UCAM-B3LYP/6-31G(d,p)) indicate that the parent **FP** has an open-shell singlet ground state, with a moderate diradical character (y_0 = 0.635) and a very small tetraradical character (y_1 = 0.003) (Table 1). The singlet triplet energy gap was calculated to be −2.3 kcal/mol, which is close to the experimental data of **FP-M**. The calculated bond lengths are similar to the X-ray crystallographic data. Bond length analysis and the calculated NICS(1)zz values indicated a typical aromatic character for rings A−C and E. On the other hand, cyclopenta ring D has a weak antiaromatic character (Figure 4c). The spin densities are evenly distributed throughout the whole π-conjugated backbone (Figure 4c), and the calculated SOMO profiles of the α and β spins of **FP** (Figure S2a) showed a typical disjoint feature.

PIF-M-ONE exhibits a slightly twisted structure (Figure 4d), and bond length analysis reveals an extended indenofluorene structure fused with two α,β-unsaturated ketone units (C1−C2, 1.392 Å; C2−C3, 1.401 Å; C3−O, 1.237 Å) (Figure 4e). It is worth noting that the oxygen was added at different positions on the phenalenyl units as compared to **HZD-M-ONE**. DFT calculations (UCAM-B3LYP/6-31G(d,p)) suggest that **PIF** also has an open-shell singlet ground state, with a moderate diradical character (y_0 = 0.351) and a small tetraradical character (y_1 = 0.031) (Table 1). The singlet−triplet energy gap was calculated to be −4.2 kcal/mol. Bond length and NICS(1)zz analysis of the ground-state singlet diradical of **PIF** indicate large aromatic character for rings E and F, weak aromatic character for rings A, C, and D, and antiaromatic character for ring B (Figure 4f). The α and β spins show a similar disjoint feature, and the spin densities are also evenly distributed throughout the whole π-conjugated backbone (Figure 4f and Figure S2b). Although **PIF** has a smaller diradical character and larger singlet−triplet energy gap than **FP**, it seems that the two terminal phenalenyl units are more prone to be attacked by oxygen and become more reactive. However, it is not clear why the reaction takes place at the site C3 rather than C1 as both have similar spin density.

DOI: 10.1021/jacs.5b12532
J. Am. Chem. Soc. 2016, 138, 1065−1077

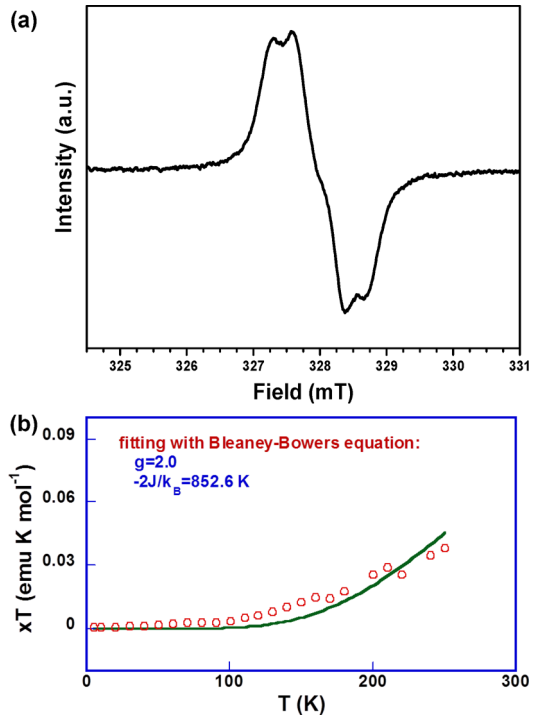

Figure 3. (a) ESR spectrum of **FP-M** in DCM solution measured at room temperature; and (b) $\chi T-T$ plot for the solid **FP-M**. The measured data were plotted as red "O", and the fitting curve was drawn using the Bleaney–Bowers equation with g_e = 2.00.

The green-color solution of **FP-M** in DCM shows a strong absorption at 836 nm (ε = 50 750 M^{-1} cm^{-1}) and several weak absorption bands with peaks at 960, 1005, and 1096 nm in the lower energy region (Figure 5a and Table 2). Similar to many

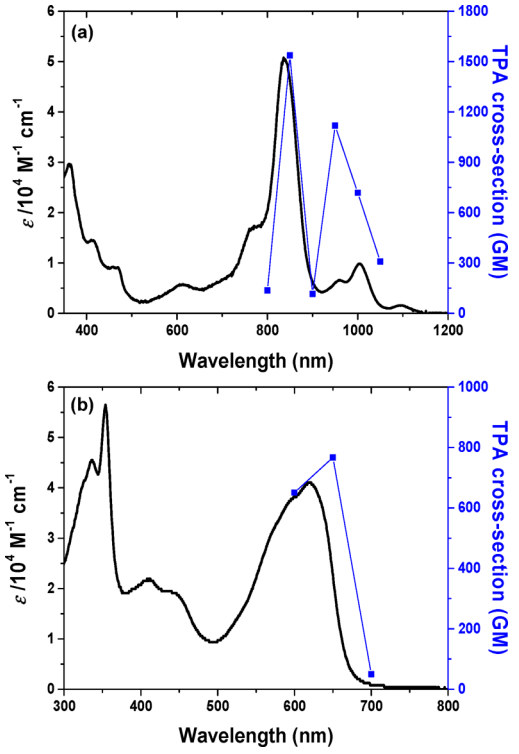

Figure 5. One-photon and two-photon absorption spectra of (a) **FP-M** and (b) **PIF-M-ONE**. TPA spectra are plotted at $\lambda_{ex}/2$.

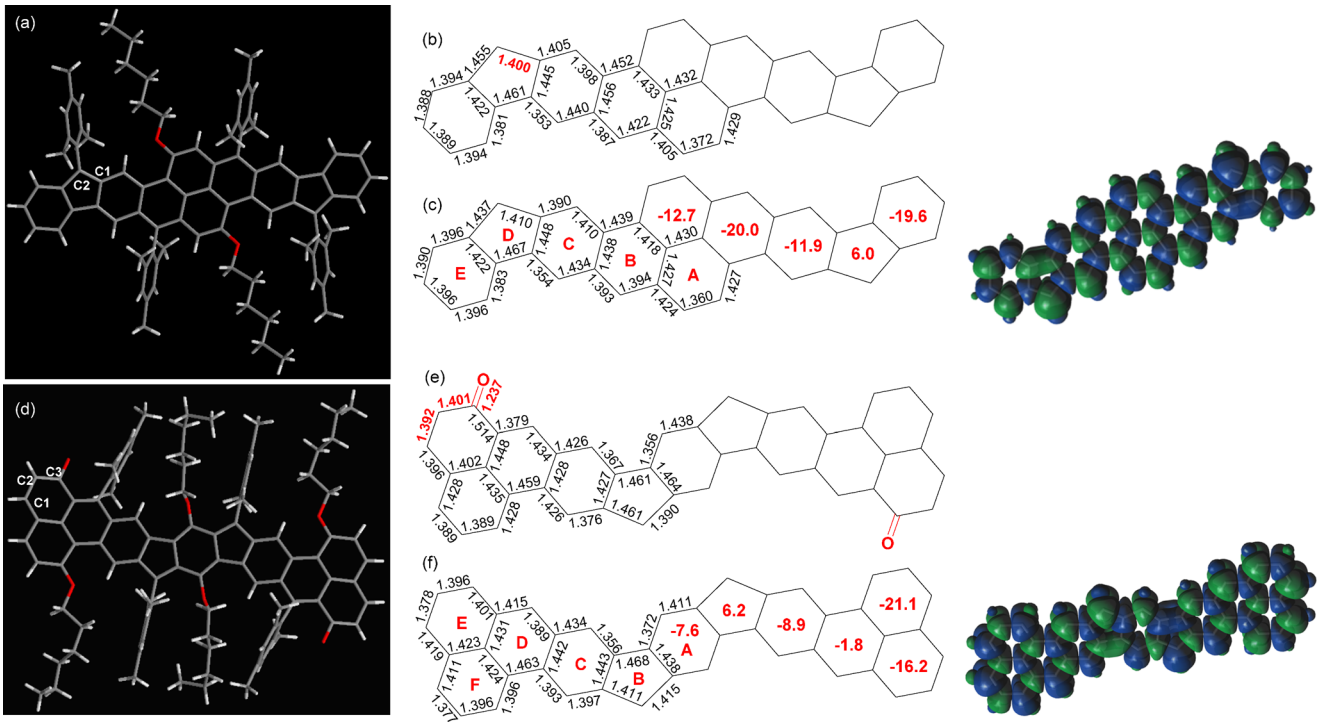

Figure 4. (a) X-ray crystallographic structure of **FP-M**; (b) selected bond lengths of the backbone of **FP-M**; (c) calculated (UCAM-B3LYP) bond lengths, NICS(1)zz values, and spin density distribution of the singlet diradical of parent **FP**; (d) X-ray crystallographic structure of **PIF-M-ONE**; (e) selected bond lengths of the backbone of **PIF-M-ONE**; and (f) calculated (UCAM-B3LYP) bond lengths, NICS(1)zz values, and spin density distribution of the singlet diradical form of the parent **PIF**.

DOI: 10.1021/jacs.5b12532
J. Am. Chem. Soc. 2016, 138, 1065–1077

Scheme 3. Synthesis of IFD-CF3, IFD-M, and IFD-F[a]

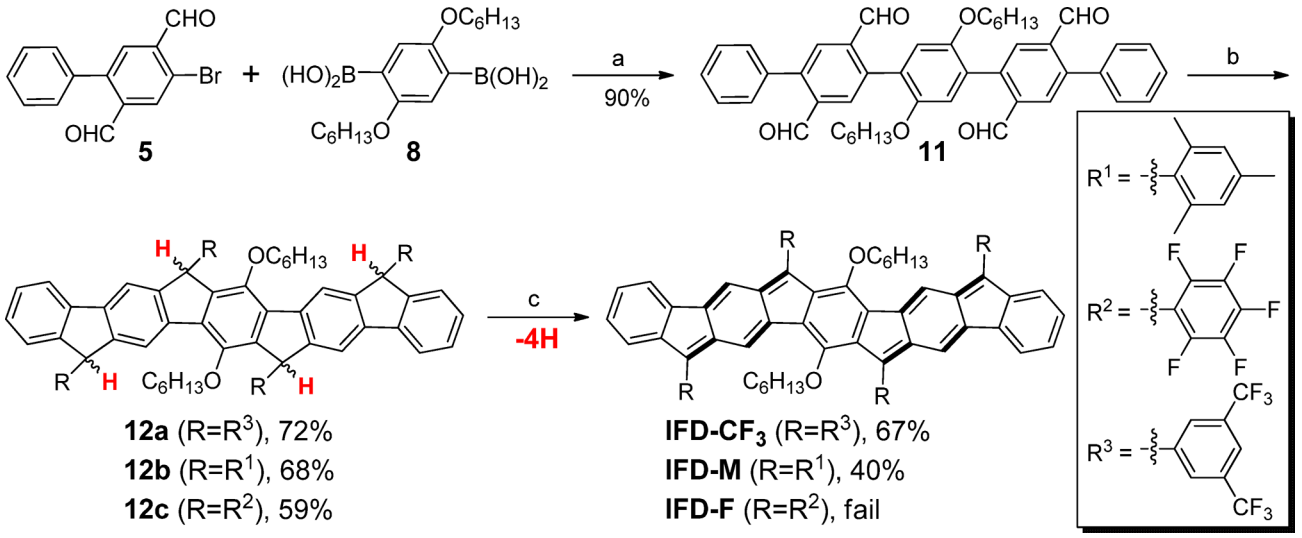

[a]Reagents and conditions: (a) $Pd(PPh_3)_4$, 2 M K_2CO_3, toluene/ethanol, 105 °C, 12 h; (b) (i) ArMgBr, Ar = mesityl, pentafluorophenyl or 3,5-bis(trifluoromethyl)phenyl, dry THF, rt, 12 h, (ii) $BF_3{\cdot}OEt_2$, dry DCM, rt, 5 min; (c) DDQ, dry toluene, reflux, 12 h.

other singlet diradicaloids, the lowest-energy absorption band likely originates from the presence of a low-lying singlet excited state dominated by a doubly excited electronic configuration (H,H→L,L).[14] It is also worth noting that the dilute solution of **FP-M** is almost transparent due to its intense and sharp near-IR absorption and weak absorption in the visible region, indicating that the **FP-M** molecule could have potential technological application as a near-IR dye.

The dioxo- product **PIF-M-ONE** shows a very different spectrum with a broad band at 620 nm (Figure 5b). In accordance with this spectrum, TD DFT calculations (B3LYP/6-31G*) predicted a strong HOMO→LUMO transition at 639.2 nm (f = 1.0033) (Figure S7b). **PIF-F-ONE** shows almost the same OPA spectrum as **PIF-M-ONE** (Figure S12b). The TA spectrum of **FP-M** exhibits a strong GSB signal around 820 nm and two ESA bands in the 450−720 and 880−950 nm region (Figure S9). The singlet excited-state lifetime was estimated to be 25 ps. The TA spectrum of **PIF-M-ONE** is similar to that of **PIF-F-ONE**. Both of them have a GSB signal around 630 nm as well as two weak ESA bands in the 450−525 and 670−850 nm region (Figure S9). Their singlet excited-state lifetimes were determined to be 7.2 and 2.2 ps, respectively. Similarly, TPA measurements were conducted, and **FP-M** exhibited a remarkable cross-section maximum value $\sigma^{(2)}_{max}$ of 1500 GM at 1700 nm, which is much larger than that for the closed-shell compounds **PIF-M-ONE** and **PIF-F-ONE** ($\sigma^{(2)}_{max}$ = 770 and 970 GM, respectively). This enhanced nonlinear optical property of **FP-M** can be explained by its moderate open-shell diradcial character.[15]

Compound **FP-M** displays well-resolved eight-stage amphoteric redox behavior with four oxidation waves at at $E_{1/2}^{ox}$ = −0.26, −0.05, 0.39, and 0.67 V and four reduction waves at $E_{1/2}^{red}$ = −1.45, −1.65, −1.84, and −2.37 V (vs Fc^+/Fc) in the CV/DPV measurements (Figure S11). The electrochemical energy gap of **FP-M** was determined as 0.94 eV, which is consistent with those obtained from the optical onset (Table 2). Compound **PIF-M-ONE** displayed two quasi-reversible oxidation waves at $E_{1/2}^{ox}$ = 0.49, 0.95 V and two reversible reduction waves at $E_{1/2}^{red}$ = −1.41, −1.59 V (vs Fc/Fc^+). On the other hand, **PIF-F-ONE** showed only one quasi-reversible oxidation wave at $E_{1/2}^{ox}$ = 0.92 V and three reversible reduction waves at $E_{1/2}^{red}$ = −1.00, −1.19, and −1.99 V due to the electron-withdrawing effect of the pentafluorophenyl substituents (Figure S11). The electrochemical energy gaps were calculated as 1.57 and 1.78 eV for **PIF-M-ONE** and **PIF-F-ONE**, respectively, which are consistent with their optical energy band gaps (Table 2).

3. 5-5-5-5 (IFD) System. To further understand the effect of the fusion mode on diradical/tetraradical characters and chemical reactivity, the 5-5-5-5 fused indenofluorene dimers were also synthesized (Scheme 3). The tetraaldehyde intermediate **11** was obtained via the Suzuki coupling between **5** and **8** in 90% yield. Treatment of **11** with aryl magnesium bromide followed by an intramolecular Friedel−Crafts alkylation reaction gave the tetrahydro-precursors **12a**/**b**/**c** with different substituents. First, the oxidative dehydrogenation of the bulky mesityl precursor **12b** with DDQ was conducted. A dark-green solid product was obtained, and the mass was matched with the target product (see the Supporting Information). However, due to the very poor solubility of the product in common organic solvents, it is difficult to do further characterization. Unfortunately, the pentafluorophenyl-substituted precursor **12c** could not be dehydrogenated by DDQ even under reflux in toluene. Finally, we found that 3,5-bis(trifluoromethyl)phenyl-substituted precursor **12a** could be easily dehydrogenated and the product **IFD-CF$_3$** has a good solubility in common solvents. The structure of **IFD-CF$_3$** was unambiguously identified by NMR, high-resolution mass spectrometry (see the Supporting Information), and X-ray crystallographic analysis.

A single crystal of **IFD-CF$_3$** was obtained via the solvent diffusion method, and its structure is shown in Figure 6a.[16] **IFD-CF$_3$** shows a fully planar backbone. The bond length analysis on the molecular backbone reveals that the bond lengths for *a* (1.392 Å) and *c* (1.365 Å) exhibit significant double-bond character, whereas bond *b* (1.431 Å) has single-bond character (Figure 6b). The large bond alternation indicates a significant contribution of the closed-shell resonance form to the ground state. DFT calculations (UCAM-B3LYP/6-31G(d,p)) predicted that the parent **IFD** has a very small

DOI: 10.1021/jacs.5b12532
J. Am. Chem. Soc. 2016, 138, 1065−1077

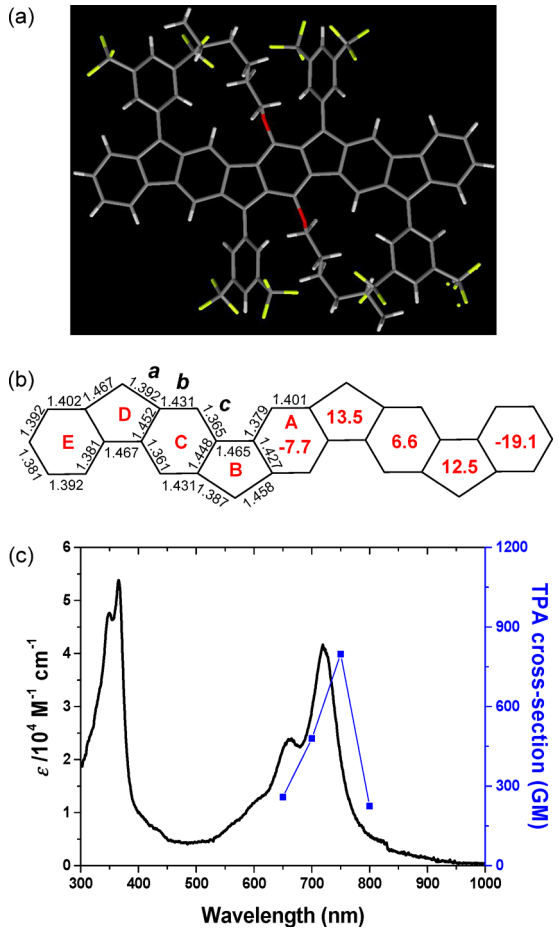

Figure 6. (a) X-ray crystallographic structure of **IFD-CF3**; (b) selected bond lengths of the backbone of **IFD-CF3**; insets are the calculated (UCAM-B3LYP) NICS(1)zz values of the parent IFD; and (c) one-photon and two-photon absorption spectra of **IFD-CF3**. TPA spectra are plotted at $\lambda_{ex}/2$.

diradical character (y_0 = 0.038) and a large singlet−triplet energy gap (ΔE_{S-T} = −8.4 kcal/mol). In accordance with this, **IFD-CF3** showed sharp NMR signals in solution, and there was no detectable ESR signal for both solution and solid. Therefore, **IFD-CF3** is better described as a closed-shell compound. NICS(1)zz calculations suggest that **IFD** can be regarded as an antiaromatic hydrocarbon in which two antiaromatic indenofluorene units are annealed together via a weak aromatic benzene ring A (Figure 6b).

The electronic absorption spectrum of **IFD-CF$_3$** in DCM showed an intense absorption band at 722 nm (ε = 41 420 M^{-1} cm^{-1}) with a long tail extending beyond 1000 nm (Figure 6c and Table 2). This spectral feature is similar to that for the antiaromatic indeno[2,1-*b*]fluorene itself containing 4*n* monocyclic conjugated π electrons. TD DFT calculations (B3LYP/6-31G*) on the closed-shell form predicted a strong HOMO→LUMO transition at 802.6 nm (f = 1.0936), which is attributable to the absorption at 722 nm, and a weak forbidden HOMO−1→LUMO transition at 890.8 nm (f = 0.0238), which can be correlated to the long tail. The TA spectrum of **IFD-CF$_3$** exhibited a strong GSB signal around 725 nm and two weak ESA bands in the 450−580 and 760−850 nm region (Figure S9). The singlet excited-state lifetime was estimated to be 3.7 ps. The TPA measurement was also conducted to investigate its nonlinear optical properties (Figure 6c and Figure S10). **IFD-CF$_3$** exhibited a cross-section $\sigma^{(2)}_{max}$ of 800 GM at 1500 nm, which is smaller than **FP-M**, presumably due to its large antiaromatic chracter. Electrochemical measurements were conducted for **IFD-CF$_3$** (Table 2 and Figure S11). Two oxidations at $E_{1/2}^{ox}$ = 0.49, 0.74 V and two reductions at $E_{red}^{1/2}$ = −1.01, −1.23 V (vs Fc/Fc$^+$) were observed. Accordingly, the electrochemical energy gap was estimated to 1.37 eV, which is close to the optical energy gap.

4. 6-6/6-5/5-5 Model Compounds and Discussion. As can be seen above, the fusion model has a significant influence on the ground-state electronic structures and chemical reactivity. To better understand the origins of this difference, three kinds of model compounds were synthesized (Figure 1 and Scheme 4). The 6-6 fused **HZ**, the 6-5 fused **PF**, and the 5-5 fused **IF** can be regarded as the model compounds for **HZD**, **FP**, and **IFD**, respectively. The dialdehyde intermediates **13**/**14** were first prepared by Suzuki coupling using the above-mentioned building blocks (see the Supporting Information). A similar reaction sequence including addition of aryl Grignard reagents, $BF_3{\cdot}Et_2O$-mediated intramolecular Friedel−Crafts alkylation, and DDQ-mediated oxidative dehydrogenation gave the desired model compounds in good yields. Compounds **IF-M** and **IF-CF3** were synthesized according to Haley's method.[4c]

Scheme 4. Synthesis of Model Compounds HZ-M/HZ-F, PF-M/PF-F, and IF-M/IF-CF$_3$[a]

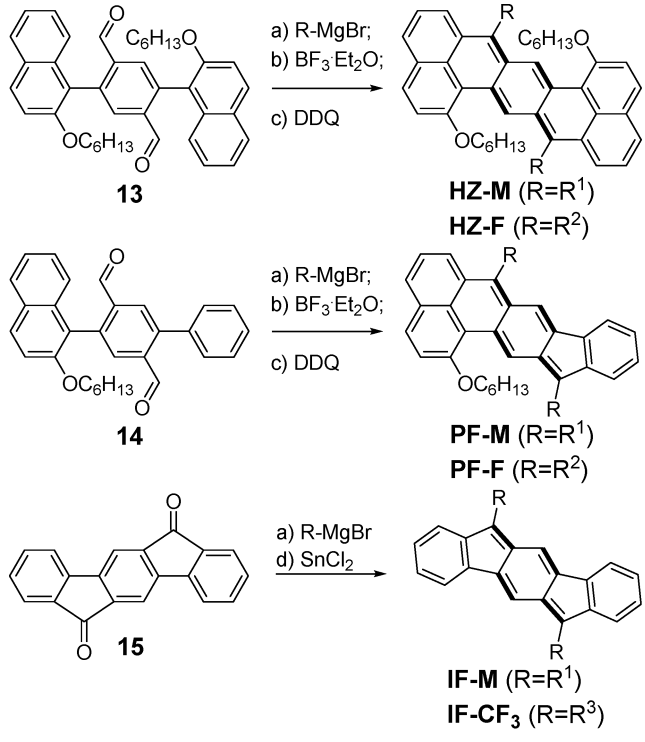

[a]Reagents and conditions: (a) R−MgBr, R = mesityl, pentafluorophenyl, or 3,5-bis(trifluoromethyl)phenyl, dry THF, rt, 12 h; (b) $BF_3{\cdot}OEt_2$, dry DCM, rt, 5 min; (c) DDQ, dry toluene, rt for **HZ-M**/**HZ-F**, **PF-M**/**PF-F**; (d) $SnCl_2$, dry toluene, 80 °C.

DOI: 10.1021/jacs.5b12532
J. Am. Chem. Soc. 2016, 138, 1065−1077

To better understand the difference between the three types of monomers, compounds **HZ-M**, **PF-M**, and **IF-M** with the same mesityl substituents were compared. The characterizations and physical properties of the other compounds are shown in the Supporting Information. All three compounds exhibit clear and sharp NMR signals, indicating their closed-shell character in the ground state. Single crystals suitable for crystallographic analysis were obtained for **HZ-M**[17] and **PF-M**[18] via solvent diffusion method, and the X-ray crystallographic structure of **IF-M** was previously reported[4a] and directly used here for comparison. Both **HZ-M** and **IF-M** exhibit a planar structure, while the unsymmetric **PF-M** shows a slightly twisted structure (Figure 7a–c). Bond length analyses

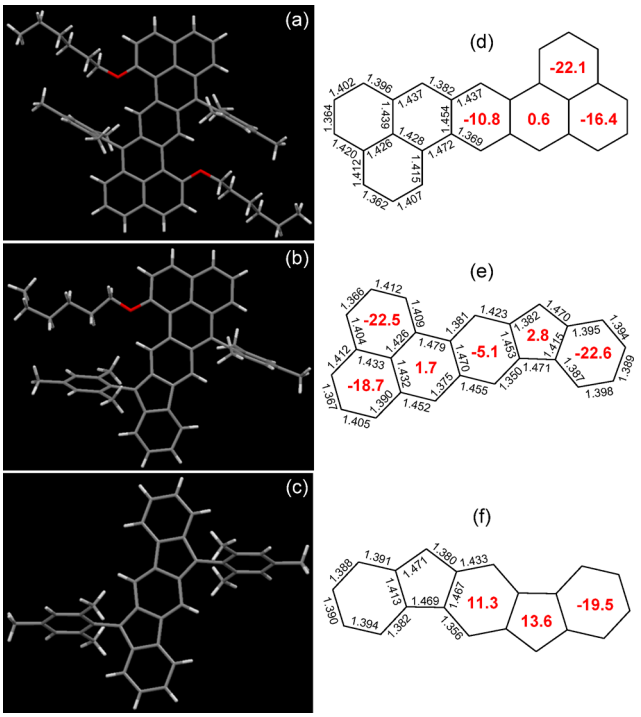

Figure 7. X-ray crystallographic structures (a–c) and selected bond lengths of the backbones (d–f) of **HZ-M**, **PF-M**, and **IF-M** (c). Insets are the calculated (UCAM-B3LYP) NICS(1)zz values of the parent **HZ**, **PF**, and **IF**.

reveal that the central *p*-QDM unit in three compounds shows large bond length alternation (Figure 7d–f), indicating their quinoidal characters. DFT calculations (UCAM-B3LYP/6-31G(d,p)) predicted that **HZ** has a small diradical character (y_0 = 0.17). On the other hand, **PF** and **IF** have a negligible diradical character (y_0 = 0.05) and a zero diradical character, respectively (Table 1). The calculated NICS(1)zz values indicate that from **HZ** through **PF** to **IF**, the central benzene ring becomes more antiaromatic (Figure 7d–f). Fundamentally, **HZ** can be regarded as a pro-aromatic system, while **IF** is an antiaromatic system, and the **PF** is in between. Looking into the resonance forms of **PF** (Figure 1f), besides the closed-shell quinoidal form and open-shell diradical form, a dipolar zwitterionic form could also contribute significantly to the ground-state structure, which may explain its smaller diradical character in comparison to **HZ**. Such a difference after incorporation of cyclopenta rings dramatically affects their ground states and physical properties.

The electronic absorption spectra of the three compounds in DCM are compared (Figure 8a). The 6-6 fused **HZ-M** displays a well-resolved spectrum with an intense p-band at 613 nm (ε = 70 030 M^{-1} cm^{-1}), which can be correlated to a HOMO→LUMO transition (λ_{abs} = 655.9 nm, f = 0.7036) based on TD DFT calculations (B3LYP/6-31G*). The 5-5 fused compound **IF-M** shows a typical absorption spectrum of antiaromatic compounds with an intense band at 515 nm (ε = 42 640 M^{-1} cm^{-1}) and a weak absorption tail extending to 700 nm. TD DFT calculations predicted an intense HOMO→LUMO transition at 518.7 nm (f = 0.5126), while the HOMO−1→LUMO transition (606.2 nm, f = 0.0) is forbidden. The similarity between the absorption spectrum of **IF-M** (also **IF-CF3**, see Figure S12) and that of **IFD-CF3** indicates both have an antiaromatic character. The unsymmetric 6-5 fused **PF-M** exhibits a very different absorption spectrum, with a moderately intense band at 436 nm (ε = 12 440 M^{-1} cm^{-1}) and a broad band extending into the near-IR region. The long-wavelength broad absorption could originate from the intramolecular charge transfer, which is very common in many unsymmetric dipolar molecular systems. Consistent with experimental results, TD DFT calculations predicted a broad absorption at 658 nm (HOMO→LUMO transition, f = 0.3826) and two close transitions at 463.1 nm (HOMO−1→LUMO transition, f = 0.1319) and 435.6 nm (HOMO→LUMO+1 transition, f = 0.1999) (Figure S7). Compounds **HZ-M**, **PF-M**, and **IF-M** also displayed distinctly different TA spectra in DCM (Figure 8b–d). The TA spectrum of **HZ-M** exhibited a GSB signal around 620 nm as well as a weak ESA band at 450–550 nm and around 820 nm (Figure 8b). The singlet excited-state lifetime was determined to be 5500 ps. Such a long excited-state lifetime could be explained by its small diradical character. **PF-M** displayed an intensive GSB signal around 630 nm and two intense ESA signals at 450–600 and 680–800 nm (Figure 8c). The singlet excited-state lifetimes was estimated to be 7.2 ps. The 5-5 fused system **IF-M** shows a GSB signal at 450–540 nm with a strong ESA signal at 550–800 nm. Because of its antiaromatic nature, it shows a very short excited-state lifetime (14 ps), similar to the alkyne-substituted indenofluorene.[19] Therefore, the singlet excited-state lifetimes dramatically decreased, and the intensity of ESA band increases going from the pro-aromatic **HZ-M** to the intermediate dipolar **PF-M** and the antiaromatic **IF-M**. The discussion in principle can go further to explain the observed phenomenon for the potential tetraradicaloid systems **HZD**, **FP**, **PIF**, and **IFD**. Similar to **HZ**, the fused dimer **HZD** can be also regarded as a pro-aromatic system. Because of the extended conjugation, the diradical character largely increases, leading to a highly reactive species. After incorporation of two cyclopenta rings, besides the closed-shell quinoidal and open-shell diradical forms, a dipolar ionic form also contributes significantly to the ground state, which results in a decrease of the diradical character as observed in **FP** and **PIF**. Reasonable stability can be achieved if the reactive sites with high spin density are appropriately protected (as seen in **FP-M**). When four cyclopenta rings are incorporated, the obtained **IFD** becomes a typical antiaromatic compound with very small diradical character, and stable materials can be obtained after kinetic blocking of the reactive sites. TPA measurements disclosed that **HZ-M** showed a larger $\sigma^{(2)}_{max}$ value (730 GM at 1200 nm) than **PF-M** (400 GM at 1300 nm) (Table 2 and Figure S10), presumably due to its larger diradical character. Because our Z-scan setup can only measure the TPA

DOI: 10.1021/jacs.5b12532
J. Am. Chem. Soc. 2016, 138, 1065–1077

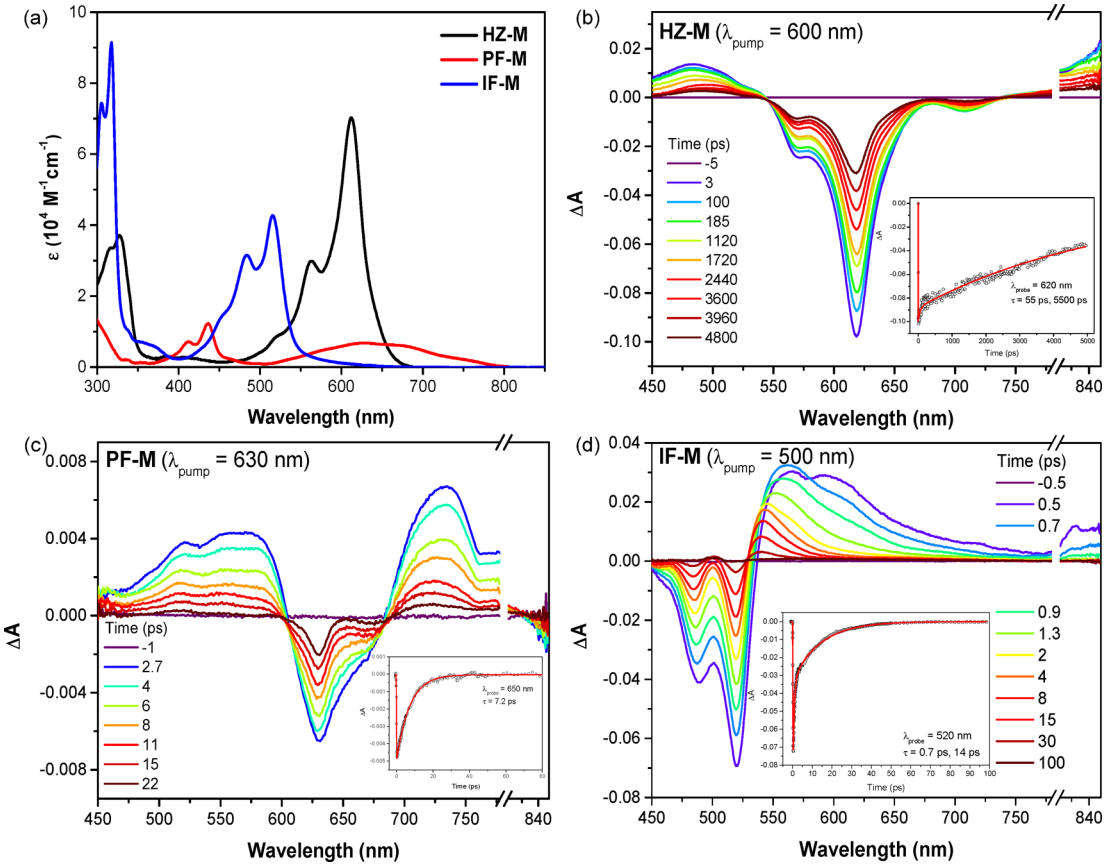

Figure 8. (a) One-photon absorption spectra of **HZ-M**, **PF-M**, and **IF-M** in DCM; and the transient absorption spectra of (a) **HZ-M**, (b) **PF-M**, and (c) **IF-M** recorded in toluene. Insets are the decay profiles.

spectrum from 1200 to 2400 nm, the TPA spectrum of **IF-M** around the 500 nm region could not be obtained.

CV and DPV measurements were conducted to study the electrochemical properties of these three model compounds **HZ-M**/**PF-M**/**IF-M** (Figure S11 and Table 2). Compound **HZ-M** gave two reversible oxidation waves at $E_{1/2}^{ox}$ = −0.27, 0.17 V and two reversible reduction waves at $E_{1/2}^{red}$ = −2.03, −2.36 V (vs Fc/Fc$^+$), while compound **IF-M** showed one oxidation wave at $E_{1/2}^{ox}$ = 0.71 V and two quasi-reversible reduction waves at $E_{1/2}^{red}$ = −1.56 and −2.07 V. The unsymmetric compound **PF-M** displays two oxidation waves at $E_{1/2}^{ox}$ = −0.07, 0.62 V and two reduction waves at −1.87, −2.37 V. The electrochemical energy gaps were determined as 1.60, 2.09, and 1.62 eV for **HZ-M**, **IF-M**, and **PF-M**, respectively, which are consistent with their optical energy band gaps (Table 2).

Although our original intention is to synthesize stable compounds with significant tetraradical character, all four systems we studied should be better described as diradicaloids because the tetraradical characters are substantially small. It seems that it is not an easy task to achieve a real tetraradical character. Nakano et al. recently calculated the polyradical characters in the linear H−H−H−H tetraradicaloid system and suggested that the diradical character (y_0) and tetraradical character (y_1) are determined by the interactions between the four spins, and moderate coupling would result in a significant tetraradical character, while unbalanced interactions would lead to a decreased tetraradical character.[20] Applied to our case, we believe that small tetraradical characters are caused by unbalanced, too strong radical−radical couplings between the four spins. Therefore, this is a key factor we must consider seriously in our future design.

III. CONCLUSIONS

We have synthesized a series of linear potential tetraradicaloids by fusion of two *p*-QDM units with aromatic benzene or naphthalene rings in different modes. Their model compounds were also prepared and compared. It turned out that the fusion mode has a dramatic effect on the ground-state electronic structures, diradical character and tetraradical characters, and chemical reactivity. The HZ dimer **HZD** has a large diradical character and is highly reactive and gave dioxo-product upon contact with air. Upon introducing two cyclopenta rings in **FP** and **PIF**, the diradical character greatly decreases. The indenofluorene dimer **IFD** with four cyclopenta rings has a very small diradical character and behaves as a closed-shell compound. These differences could be explained by the pro-aromatic/antiaromatic character of the molecules and the intramolecular charge transfer effect based on the model compound studies. Because of unbalanced radical−radical interactions, these compounds exhibited small tetraradical character and are better described as diradicaloids with tunable diradical character. Our comprehensive studies provide insight into the design and synthesis of stable open-shell singlet polyradicaloids in the future.

■ ASSOCIATED CONTENT

Supporting Information

The Supporting Information is available free of charge on the ACS Publications website at DOI: 10.1021/jacs.5b12532.

DOI: 10.1021/jacs.5b12532
J. Am. Chem. Soc. 2016, 138, 1065−1077

Synthetic procedures and characterization data of all other new compounds; details for all physical characterizations and theoretical calculations; and additional spectroscopic and X-ray crystallographic data (PDF)
X-ray data for compound (CIF)
X-ray data for compound (CIF)
X-ray data for compound (CIF)
X-ray data for compound (CIF)
X-ray data for compound (CIF)
X-ray data for compound (CIF)
X-ray data for compound (CIF)

AUTHOR INFORMATION

Corresponding Authors

*msedingj@nus.edu.sg
*dongho@yonsei.ac.kr
*chmwuj@nus.edu.sg

Notes

The authors declare no competing financial interest.

ACKNOWLEDGMENTS

J.W. acknowledges financial support from the MOE Tier 3 programme (MOE2014-T3-1-004), MOE Tier 2 grant (MOE2014-T2-1-080), and A*STAR JCO grant (1431AFG100). This work at Yonsei University was supported by the Global Frontier R&D Program on Center for Multiscale Energy System funded by the National Research Foundation under the Ministry of Science, ICT & Future, Korea (NRF-2014M3A6A7060583). H.Y. and N.A. acknowledge the financial support by Grants-in-Aid for Scientific Research (KAKENHI) nos. 25288092, 26620167, 26105004, and 26288038 from the Japan Society for the Promotion of Science (JSPS). K.-W.H. is thankful for financial support from KAUST. We thank Dr. Bruno Donnadieu for crystallographic analysis on some samples. We thank Professor Michael Haley (University of Oregon) and Professor Yoshito Tobe (Osaka University) for helpful discussions.

REFERENCES

(1) (a) Rajca, A. *Chem. Rev.* **1994**, *94*, 871. (b) Morita, Y.; Suzuki, K.; Sato, S.; Takui, T. *Nat. Chem.* **2011**, *3*, 197. (c) Sun, Z.; Ye, Q.; Chi, C.; Wu, J. *Chem. Soc. Rev.* **2012**, *41*, 7857. (d) Shimizu, A.; Hirao, Y.; Kubo, T.; Nakano, M.; Botek, E.; Champagne, B. *AIP Conf. Proc.* **2009**, *1504*, 399. (e) Sun, Z.; Zeng, Z.; Wu, J. *Chem. - Asian J.* **2013**, *8*, 2894. (f) Abe, M. *Chem. Rev.* **2013**, *113*, 7011. (g) Sun, Z.; Zeng, Z.; Wu, J. *Acc. Chem. Res.* **2014**, *47*, 2582. (h) Nakano, M. *Excitation Energies and Properties of Open-Shell Singlet Molecules*; Springer: New York, 2014. (i) Kubo, T. *Chem. Rec.* **2015**, *15*, 218. (j) Zeng, Z.; Shi, X. L.; Chi, C.; López Navarrete, J. T.; Casado, J.; Wu, J. *Chem. Soc. Rev.* **2015**, *44*, 6578. (k) Kubo, T. *Chem. Lett.* **2015**, *44*, 111. (l) Miyoshi, H.; Nobusue, S.; Shimizu, A.; Tobe, Y. *Chem. Soc. Rev.* **2015**, *44*, 6560.

(2) (a) Ohashi, K.; Kubo, T.; Masui, T.; Yamamoto, K.; Nakasuji, K.; Takui, T.; Kai, Y.; Murata, I. *J. Am. Chem. Soc.* **1998**, *120*, 2018. (b) Kubo, T.; Sakamoto, M.; Akabane, M.; Fujiwara, Y.; Yamamoto, K.; Akita, M.; Inoue, K.; Takui, T.; Nakasuji, K. *Angew. Chem., Int. Ed.* **2004**, *43*, 6474. (c) Kubo, T.; Shimizu, A.; Sakamoto, M.; Uruichi, M.; Yakushi, K.; Nakano, M.; Shiomi, D.; Sato, K.; Takui, T.; Morita, Y.; Nakasuji, K. *Angew. Chem., Int. Ed.* **2005**, *44*, 6564. (d) Shimizu, A.; Uruichi, M.; Yakushi, K.; Matsuzaki, H.; Okamoto, H.; Nakano, M.; Hirao, Y.; Matsumoto, K.; Kurata, H.; Kubo, T. *Angew. Chem., Int. Ed.* **2009**, *48*, 5482. (e) Shimizu, A.; Kubo, T.; Uruichi, M.; Yakushi, K.; Nakano, M.; Shiomi, D.; Sato, K.; Takui, T.; Hirao, Y.; Matsumoto, K.; Kurata, H.; Morita, Y.; Nakasuji, K. *J. Am. Chem. Soc.* **2010**, *132*, 14421. (f) Shimizu, A.; Hirao, Y.; Matsumoto, K.; Kurata, H.; Kubo, T.; Uruichi, M.; Yakushi, K. *Chem. Commun.* **2012**, *48*, 5629.

(3) (a) Umeda, R.; Hibi, D.; Miki, K.; Tobe, Y. *Org. Lett.* **2009**, *11*, 4104. (b) Wu, T. C.; Chen, C. H.; Hibi, D.; Shimizu, A.; Tobe, Y.; Wu, Y. T. *Angew. Chem., Int. Ed.* **2010**, *49*, 7059. (c) Sun, Z.; Huang, K.-W.; Wu, J. *Org. Lett.* **2010**, *12*, 4690. (d) Sun, Z.; Huang, K.-W.; Wu, J. *J. Am. Chem. Soc.* **2011**, *133*, 11896. (e) Li, Y.; Heng, W.-K.; Lee, B. S.; Aratani, N.; Zafra, J. L.; Bao, N.; Lee, R.; Sung, Y. M.; Sun, Z.; Huang, K.-W.; Webster, R. D.; López Navarrete, J. T.; Kim, D.; Osuka, A.; Casado, J.; Ding, J.; Wu, J. *J. Am. Chem. Soc.* **2012**, *134*, 14913. (f) Zeng, W.; Ishida, M.; Lee, S.; Sung, Y.; Zeng, Z.; Ni, Y.; Chi, C.; Kim, D.-H.; Wu, J. *Chem. - Eur. J.* **2013**, *19*, 16814. (g) Sun, Z.; Lee, S.; Park, K.; Zhu, X.; Zhang, W.; Zheng, B.; Hu, P.; Zeng, Z.; Das, S.; Li, Y.; Chi, C.; Li, R.; Huang, K.; Ding, J.; Kim, D.; Wu, J. *J. Am. Chem. Soc.* **2013**, *135*, 18229. (h) Sun, Z.; Wu, J. *J. Org. Chem.* **2013**, *78*, 9032. (i) Shan, L.; Liang, Z.-X.; Xu, X.-M.; Tang, Q.; Miao, Q. *Chem. Sci.* **2013**, *4*, 3294. (j) Zafra, J. L.; González Cano, R. C.; Delgado, M. C. R.; Sun, Z.; Li, Y.; López Navarrete, J. T.; Wu, J.; Casado, J. *J. Chem. Phys.* **2014**, *140*, 054706. (k) Li, Y.; Huang, K.-W.; Sun, Z.; Webster, R. D.; Zeng, Z.; Zeng, W. D.; Chi, C.; Furukawa, K.; Wu, J. *Chem. Sci.* **2014**, *5*, 1908. (l) Das, S.; Lee, S.; Son, M.; Zhu, X.; Zhang, W.; Zheng, B.; Hu, P.; Zeng, Z.; Sun, Z.; Zeng, W.; Li, R.-W.; Huang, K.-W.; Ding, J.; Kim, D.; Wu, J. *Chem. - Eur. J.* **2014**, *20*, 11410. (m) Sun, Z.; Zheng, B.; Hu, P.; Huang, K.-W.; Wu, J. *ChemPlusChem* **2014**, *79*, 1549. (n) Shi, X.; Lee, S.; Son, M.; Zheng, B.; Chang, J.; Jing, L.; Huang, K.-W.; Kim, D.; Chi, C. *Chem. Commun.* **2015**, *51*, 13138.

(4) (a) Chase, D. T.; Rose, B. D.; McClintock, S. P.; Zakharov, L. N.; Haley, M. M. *Angew. Chem., Int. Ed.* **2011**, *50*, 1127. (b) Shimizu, A.; Tobe, Y. *Angew. Chem., Int. Ed.* **2011**, *50*, 6906. (c) Chase, D. T.; Fix, A. G.; Kang, S. J.; Rose, B. D.; Weber, C. D.; Zhong, Y.; Zakharov, L. N.; Lonergan, M. C.; Nuckolls, C.; Haley, M. M. *J. Am. Chem. Soc.* **2012**, *134*, 10349. (d) Fix, A. G.; Deal, P. E.; Vonnegut, C. L.; Rose, B. D.; Zakharov, L. N.; Haley, M. M. *Org. Lett.* **2013**, *15*, 1362. (e) Rose, B. D.; Vonnegut, C. L.; Zakharov, L. N.; Haley, M. M. *Org. Lett.* **2012**, *14*, 2426. (f) Shimizu, A.; Kishi, R.; Nakano, M.; Shiomi, D.; Sato, K.; Takui, T.; Hisaki, I.; Miyata, M.; Tobe, Y. *Angew. Chem., Int. Ed.* **2013**, *52*, 6076. (g) Fix, A. G.; Chase, D. T.; Haley, M. M. *Top. Curr. Chem.* **2012**, *349*, 159. (h) Miyoshi, H.; Nobusue, S.; Shimizu, A.; Hisaki, I.; Miyatab, M.; Tobe, Y. *Chem. Sci.* **2014**, *5*, 163. (i) Young, B. S.; Chase, D. T.; Marshall, J. L.; Vonnegut, C. L.; Zakharov, L. N.; Haley, M. M. *Chem. Sci.* **2014**, *5*, 1008. (j) Luo, D.; Lee, S.; Zheng, B.; Sun, Z.; Zeng, W.; Huang, K.-W.; Furukawa, K.; Kim, D.; Webster, R. D.; Wu, J. *Chem. Sci.* **2014**, *5*, 4944.

(5) Konishi, A.; Hirao, Y.; Nakano, M.; Shimizu, A.; Botek, E.; Champagne, B.; Shiomi, D.; Sato, K.; Takui, T.; Matsumoto, K.; Kurata, H.; Kubo, T. *J. Am. Chem. Soc.* **2010**, *132*, 11021. (b) Konishi, A.; Hirao, Y.; Matsumoto, K.; Kurata, H.; Kishi, R.; Shigeta, Y.; Nakano, M.; Tokunaga, K.; Kamada, K.; Kubo, T. *J. Am. Chem. Soc.* **2013**, *135*, 1430.

(6) (a) Zhu, X.; Tsuji, H.; Nakabayashi, H.; Ohkoshi, S.; Nakamura, E. *J. Am. Chem. Soc.* **2011**, *133*, 16342. (b) Zeng, Z.; Sung, Y. M.; Bao, N.; Tan, D.; Lee, R.; Zafra, J. L.; Lee, B. S.; Ishida, M.; Ding, J.; López Navarrete, J. T.; Li, Y.; Zeng, W.; Kim, D.; Huang, K.-W.; Webster, R. D.; Casado, J.; Wu, J. *J. Am. Chem. Soc.* **2012**, *134*, 14513. (c) Zeng, Z.; Ishida, M.; Zafra, J. L.; Zhu, X.; Sung, Y. M.; Bao, N.; Webster, R. D.; Lee, B. S.; Li, R.-W.; Zeng, W.; Li, Y.; Chi, C.; López Navarrete, J. T.; Ding, J.; Casado, J.; Kim, D.; Wu, J. *J. Am. Chem. Soc.* **2013**, *135*, 6363. (d) Zeng, Z.; Lee, S.; Zafra, J. L.; Ishida, M.; Zhu, X.; Sun, Z.; Ni, Y.; Webster, R. D.; Li, R.-W.; López Navarrete, J. T.; Chi, C.; Ding, J.; Casado, J.; Kim, D.; Wu, J. *Angew. Chem., Int. Ed.* **2013**, *52*, 8561. (e) Zeng, Z.; Lee, S.; Zafra, J. L.; Ishida, M.; Bao, N.; Webster, R. D.; López Navarrete, J. T.; Ding, J.; Casado, J.; Kim, D.-H.; Wu, J. *Chem. Sci.* **2014**, *5*, 3072. (f) Zeng, Z.; Wu, J. *Chem. Rec.* **2015**, *15*, 322. (g) Zeng, Z.; Lee, S.; Son, M.; Fukuda, K.; Burrezo, P. M.; Zhu, X.; Qi, Q.; Li, R.-W.; López Navarrete, J. T.; Ding, J.; Casado, J.; Nakano, M.; Kim, D.; Wu, J. *J. Am. Chem. Soc.* **2015**, *137*, 8572. (h) Lim, Z. L.; Zheng, B.; Huang, K.-W.; Liu, Y.; Wu, J. *Chem. - Eur. J.* **2015**, *21*, 18724.

DOI: 10.1021/jacs.5b12532
J. Am. Chem. Soc. 2016, 138, 1065−1077

(7) Nobusue, S.; Miyoshi, H.; Shimizu, A.; Hisaki, I.; Fukuda, K.; Nakano, M.; Tobe, Y. *Angew. Chem., Int. Ed.* **2015**, *54*, 2090.
(8) (a) Smet, M.; Shukla, R.; Fülöp, L.; Dehaen, W. *Eur. J. Org. Chem.* **1998**, *1998*, 2769. (b) Smet, M.; Van Dijk, J.; Dehaen, W. *Synlett* **1999**, *1999*, 495. (c) Wegner, H. A.; Scott, L. T.; de Meijere, A. *J. Org. Chem.* **2003**, *68*, 883. (d) Mohebbi, A. R.; Yuen, J.; Fan, J.; Munoz, C.; Wang, M.; Shirazi, R. S.; Seifter, J.; Wudl, F. *Adv. Mater.* **2011**, *23*, 4644. (e) Mohebbi, A. R.; Wudl, F. *Chem. - Eur. J.* **2011**, *17*, 2642. (f) Eversloh, C. L.; Avlasevich, Y.; Li, C.; Müllen, K. *Chem. - Eur. J.* **2011**, *17*, 12756. (g) Wood, J. D.; Jellison, J. L.; Finke, A. D.; Wang, L.; Plunkett, K. N. *J. Am. Chem. Soc.* **2012**, *134*, 15783. (h) Xia, H.; Liu, D.; Xu, X.; Miao, Q. *Chem. Commun.* **2013**, *49*, 4301. (i) Lakshminarayana, A. N.; Chang, J.; Luo, J.; Zheng, B.; Huang, K.-W.; Chi, C. *Chem. Commun.* **2015**, *51*, 3604.
(9) (a) Scherf, U.; Müllen, K. *Polymer* **1992**, *33*, 2443. (b) Kertesz, M. *Macromolecules* **1995**, *28*, 1475. (c) Tobe, Y. *Chem. Rec.* **2015**, *15*, 86.
(10) Crystallographic data for **HZD-M-ONE**: $C_{106}H_{110}O_6$, M_w = 1480.04; monoclinic; space group $P\bar{1}$; a = 15.7254(8) Å, b = 16.3000(8) Å, c = 19.7644(10) Å, α = 88.0843(9)°, β = 73.1877(9)°, γ = 70.5165(9)°; V = 4560.7(4) Å^3; Z = 2; ρ_{calcd} = 1.252 Mg/m^3; R1 = 0.0640 ($I > 2\sigma(I)$), wR2 = 0.1934 (all data). CCDC no.: 1436511.
(11) Bleaney, B.; Bowers, K. D. *Proc. R. Soc. London, Ser. A* **1952**, *214*, 451.
(12) Crystallographic structures for **FP-M**: $C_{86}H_{84}O_2$, M_w = 1148.65; monoclinic; space group $P2(1)/c$; a = 9.2447(4) Å, b = 27.6365(10) Å, c = 14.8907(5) Å, α = 90°, β = 98.658(3)°, γ = 90°; V = 3761.1(2) Å^3; Z = 4; ρ_{calcd} = 1.178 Mg/m^3; R1 = 0.0530 ($I > 2\sigma(I)$), wR2 = 0.1368 (all data). CCDC no.: 1434045.
(13) Crystallographic structures for **PIF-M-ONE**: $C_{102}H_{110}O_6$, M_w = 1430.83; triclinic; space group $P\bar{1}$; a = 10.9480(4) Å, b = 12.0802(4) Å, c = 16.2323(6) Å, α = 69.553(2)°, β = 76.264(2)°, γ = 79.814(2)°; V = 1943.58(12) Å^3; Z = 1; ρ_{calcd} = 1.222 Mg/m^3; R1 = 0.0570 ($I > 2\sigma(I)$), wR2 = 0.1578 (all data). CCDC no.: 1436512.
(14) Motta, S. D.; Negri, F.; Fazzi, D.; Castiglioni, C.; Canesi, E. V. *J. Phys. Chem. Lett.* **2010**, *1*, 3334.
(15) Nakano, M.; Nagao, H.; Yamaguchi, K. *Phys. Rev. A: At., Mol., Opt. Phys.* **1997**, *55*, 1503. (b) Nakano, M.; Kishi, R.; Nitta, T.; Kubo, T.; Nakasuji, K.; Kamada, K.; Ohta, K.; Champagne, B.; Botek, E.; Yamaguchi, K. *J. Phys. Chem. A* **2005**, *109*, 885. (c) Nakano, M.; Kubo, T.; Kamada, K.; Ohta, K.; Kishi, R.; Ohta, S.; Nakagawa, N.; Takahashi, H.; Furukawa, S.; Morita, Y.; Nakasuji, K.; Yamaguchi, K. *Chem. Phys. Lett.* **2006**, *418*, 142. (d) Ohta, S.; Nakano, M.; Kubo, K.; Kamada, K.; Ohta, K.; Kishi, R.; Nakagawa, N.; Champagne, B.; Botek, E.; Takebe, A.; Umezaki, S.; Nate, M.; Takahashi, H.; Furukawa, S.; Morita, Y.; Nakasuji, K.; Yamaguchi, K. *J. Phys. Chem. A* **2007**, *111*, 3633. (e) Nakano, M.; Kishi, R.; Takebe, A.; Nate, M.; Takahashi, H.; Kubo, T.; Kamada, K.; Ohta, K.; Champagne, B.; Botek, E. *Comput. Lett.* **2007**, *3*, 333. (f) Nakano, M.; Kishi, R.; Ohta, S.; Takahashi, H.; Kubo, T.; Kamada, K.; Ohta, K.; Botek, E.; Champagne, B. *Phys. Rev. Lett.* **2007**, *99*, 033001. (g) Nakano, M.; Nagai, H.; Fukui, H.; Yoneda, K.; Kishi, R.; Takahashi, H.; Shimizu, A.; Kubo, T.; Kamada, K.; Ohta, K.; Champagne, B.; Botek, E. *Chem. Phys. Lett.* **2008**, *467*, 120. (h) Yoneda, K.; Nakano, M.; Inoue, Y.; Inui, T.; Fukuda, K.; Shigeta, Y.; Kubo, T.; Champagne, B. *J. Phys. Chem. C* **2012**, *116*, 17787. (i) Nakano, M.; Champagne, B. *Theor. Chem. Acc.* **2015**, *134*, 23−1−9.
(16) Crystallographic structures for **IFD-CF3**: $C_{78}H_{50}F_{24}O_2$, M_w = 1475.22; monoclinic; space group $C2/c$; a = 32.7089(12) Å, b = 14.2715(5) Å, c = 15.6260(6) Å, α = 90°, β = 104.233(2)°, γ = 90°; V = 7070.4(5) (12) Å^3; Z = 8; ρ_{calcd} = 1.386 Mg/m^3; R1 = 0.1243 ($I > 2\sigma(I)$), wR2 = 0.3981 (all data). CCDC no.: 1434047.
(17) Crystallographic structures for **HZ-M**: $C_{58}H_{60}O_2$, M_w = 789.06; monoclinic; space group $C2/c$; a = 26.3642(16) Å, b = 16.1386(9) Å, c = 23.420(2) Å, α = 90°, β = 119.4610(18)°, γ = 90°; V = 8676.1(11) Å^3; Z = 8; ρ_{calcd} = 1.208 Mg/m^3; R1 = 0.0513 ($I > 2\sigma(I)$), wR2 = 0.1481 (all data). CCDC no.: 1436513.
(18) Crystallographic structures for **PF-M**: $C_{48}H_{46}O$, M_w = 638.90; monoclinic; space group $P2(1)/n$; a = 14.9865(5) Å, b = 7.9786(3) Å, c = 34.6321(12) Å, α = 90°, β = 101.364(2)°, γ = 90°; V = 4059.8(2) Å^3; Z = 4; ρ_{calcd} = 1.196 Mg/m^3; R1 = 0.0497 ($I > 2\sigma(I)$), wR2 = 0.1335 (all data). CCDC no.: 1434048.
(19) Rose, B. D.; Shoer, L. E.; Wasielewski, M. R.; Haley, M. M. *Chem. Phys. Lett.* **2014**, *616*−*617*, 137.
(20) Nakano, M.; Minami, T.; Fukui, H.; Kishi, R.; Shigeta, Y.; Champagne, B. *J. Chem. Phys.* **2012**, *136*, 024315.
(21) Crystallographic structures for **HZ-F**: $C_{52}H_{38}F_{10}O_2$, M_w = 884.86; triclinic; space group $P\bar{1}$; a = 7.7536(3) Å, b = 8.4647(4) Å, c = 16.2224(8) Å, α = 83.656(2)°, β = 80.330(2)°, γ = 65.6020(10)°; V = 954.85(8) Å^3; Z = 2; ρ_{calcd} = 1.539 Mg/m^3; R1 = 0.0457 ($I > 2\sigma(I)$), wR2 = 0.1282 (all data). CCDC no.: 1434046.

DOI: 10.1021/jacs.5b12532
J. Am. Chem. Soc. 2016, 138, 1065−1077